Check for updates

Geophysical Research Letters

RESEARCH LETTER
10.1029/2025GL117229

Receiver Function Imaging of the Mantle Transition Zone Beneath the East Sayan Mountains and Adjacent Area in Central Asia: Implications for Lithospheric Drip and Intraplate Cenozoic Volcanism

Yangyang Liao[1], Kelly H. Liu[1], and Stephen S. Gao[1]

[1]Department of Earth Sciences and Engineering, Missouri University of Science and Technology, Rolla, MO, USA

Key Points:

- Results suggest ancient slab remnants in the lower mantle transition zone, and slab dehydration led to volcanism in peripheral area
- Thinning of the mantle transition zone in the Tuva-Mongolian Massif is likely caused by mantle upwelling induced by slab subduction
- Depth variation of the 410 and 660 km discontinuities is attributable to a lithospheric drip beneath the East Sayan Mountains

Supporting Information:

Supporting Information may be found in the online version of this article.

Correspondence to:

S. S. Gao,
sgao@mst.edu

Citation:

Liao, Y., Liu, K. H., & Gao, S. S. (2025). Receiver function imaging of the mantle transition zone beneath the East Sayan Mountains and adjacent area in central Asia: Implications for lithospheric drip and intraplate Cenozoic volcanism. *Geophysical Research Letters*, *52*, e2025GL117229. https://doi.org/10.1029/2025GL117229

Received 2 JUN 2025
Accepted 22 JUL 2025

Author Contributions:

Conceptualization: Yangyang Liao, Kelly H. Liu, Stephen S. Gao
Data curation: Yangyang Liao, Stephen S. Gao
Formal analysis: Yangyang Liao, Stephen S. Gao
Funding acquisition: Kelly H. Liu
Investigation: Yangyang Liao, Stephen S. Gao
Methodology: Yangyang Liao, Kelly H. Liu, Stephen S. Gao
Project administration: Kelly H. Liu, Stephen S. Gao
Resources: Yangyang Liao, Kelly H. Liu, Stephen S. Gao

© 2025. The Author(s).
This is an open access article under the terms of the Creative Commons Attribution License, which permits use, distribution and reproduction in any medium, provided the original work is properly cited.

Abstract To provide constraints on the formation mechanisms of intracontinental volcanisms and intriguing lithospheric thickness variations in the East Sayan Mountains and surrounding areas, we stack P-to-s receiver functions to image the 410-km and 660-km discontinuities. Mantle transition zone (MTZ) thickening observed in a continuous area is attributable to ancient slab remnants, and Cenozoic volcanisms in the peripheral area can be explained by slab dehydration. The thinning of the MTZ in the Tuva-Mongolian Massif can be explained by mantle upwelling branches induced by slab subduction. Our results reveal an approximately circular area in the MTZ that is significantly thicker than usual, suggesting the presence of detached mantle lithosphere in the form of a lithospheric drip extending to the MTZ. The presence of the drip is consistent with geochemical and lithospheric thickness observations, and the drip could be triggered by passage of a mantle plume currently located beneath western Lake Baikal.

Plain Language Summary The depths of the upper and lower boundaries of the mantle transition zone serve as indicators of in situ temperature changes, velocity anomalies, and water content. To understand the tectonic processes and origin of volcanic activities beneath the East Sayan Mountains and adjacent areas, we analyze seismic waves to examine the depth variations of the boundaries. Our findings reveal a thickened mantle transition zone in the central part of the study area, which we link to Paleo-slab remnants. The volcanic activities could be associated with the dehydration of the subducted slab segments in the mantle transition zone. The thinner than normal mantle transition zone observed underneath the Tuva-Mongolian Massif may result from upwelling triggered by the sinking of the slab remnants. Additionally, a thickened mantle transition zone beneath the Sayan Mountains suggests a lithospheric drip, possibly induced by the passage of a hot mantle plume currently sitting beneath western Lake Baikal.

1. Introduction

The dripping of Earth's lithosphere is caused by gravitational instability and is responsible for a variety of tectonic processes, including volcanic activity, variations in surface topography and crustal thickness, thickening of the mantle lithosphere in the central portion and thinning in the peripheral area of the lithospheric drip (e.g., DeCelles et al., 2015; Furman et al., 2016; Göğüş & Pysklywec, 2008; McMillan & Schoenbohm, 2023; West et al., 2009). Gravitational instability occurs when the lithosphere achieves negative buoyancy, which can arise from several mechanisms: (a) thermal contraction and thickening of the lithosphere (Conrad & Molnar, 1997; Houseman et al., 1981), (b) metasomatic alteration of the lithosphere, resulting in the enrichment of high-density mineral phases such as garnet and pyroxene (Furman et al., 2016; Kay & Kay, 1993), and (c) volcanic activities leading to the formation of an anomalously thick and dense crustal layer (Ducea & Saleeby, 1998; Rapp & Watson, 1995). Mantle plumes can also initiate the downwelling of mantle lithosphere by decreasing the density of the sub-lithospheric mantle and weakening the lithosphere due to high temperature (Camp & Hanan, 2008; Furman et al., 2016; Hales et al., 2005). Thermal influence from the mantle plume can destabilize the dense and meta-somatized lower lithosphere, leading to a drip effect and generating melting processes associated with mafic magmatism (Furman et al., 2016). Globally, the majority of the suggested lithospheric drips are situated in the vicinity of currently active convergent margins (e.g., Boyd et al., 2004; McMillan & Schoenbohm, 2023; Zandt, 2003). To date, lithospheric drips resulting from interactions between mantle plumes and thickened lithosphere have been rarely observed. This study provides geophysical evidence consistent with a lithospheric drip possibly triggered by the transit of thick lithosphere over a mantle plume.

Software: Yangyang Liao, Kelly H. Liu, Stephen S. Gao
Supervision: Kelly H. Liu, Stephen S. Gao
Validation: Yangyang Liao, Stephen S. Gao
Visualization: Yangyang Liao, Stephen S. Gao
Writing – original draft: Yangyang Liao, Stephen S. Gao
Writing – review & editing: Yangyang Liao, Kelly H. Liu, Stephen S. Gao

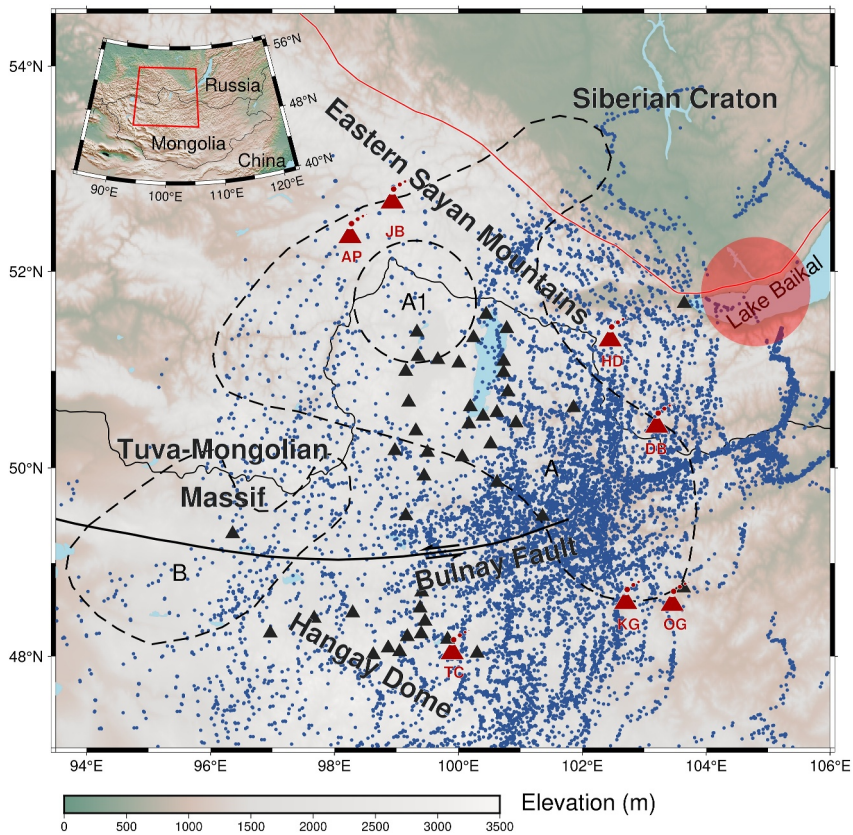

Figure 1. Topographic relief map of the East Sayan and northern Mongolia showing the locations of broadband seismic stations used in the study (black triangles) and Cenozoic volcanoes (red triangles). Blue dots show the ray-piecing points at 535 km depth. JB, Jom-Bolok, AP, Azas Plateau, HD, Hamar-Daban Range, DB, Dgida Basin, KG, Khanuy Gol, OG, Orkhon Gol, and TC, Taryat Chulutu. The thick solid black line indicates the Bulnay fault, and the solid red line represents the tectonic boundary of the Siberian Craton. Dashed lines delineate the subareas in this study, and the red circle represents the approximate horizontal extent of a tomography-revealed plume stem in the upper mantle (Wu et al., 2021).

Depth variations of the 410 and 660 km discontinuities (d410 and d660) defining the mantle transition zone (MTZ) have been widely used to provide independent constraints on the lateral and vertical distributions of seismic velocities, as well as associated thermal and water-content anomalies in the upper mantle and MTZ (e.g., S. S. Gao & Liu, 2014b; Gu et al., 1998; Shearer, 1991). In an olivine dominated system, which is commonly found beneath relatively stable continental areas, the mineral phase transitions occurring at the d410 and d660 are from olivine to wadsleyite and from ringwoodite to bridgmanite (Mg perovskite + magnesiowustite), respectively (Ito & Katsura, 1989; Ringwood, 1975; Yamazaki & Karato, 2001). The correlation between temperature and pressure under which these phase transitions take place can be described by the Clapeyron slopes (Bina & Helffrich, 1994; Fei et al., 2004; Helffrich, 2000). In areas with lower-than-normal MTZ temperatures such as those associated with subducted slab segments, the positive and negative Clapeyron slopes for the d410 and d660, respectively, lead to a thicker than normal MTZ. Conversely, positive thermal anomalies, such as those accompanying thermal upwelling, result in a depressed d410 and an uplifted d660, leading to a thinner than normal MTZ. Additionally, water-enriched peridotite or a large amount of water in the MTZ also plays a role in affecting the topography of the MTZ discontinuities, resulting in thicker than normal MTZ (Smyth & Frost, 2002; van der Meijde et al., 2003; Wood et al., 1996).

2. Tectonic Setting

The East Sayan Mountains and northern Mongolian Plateau (Figure 1) are characterized by a high elevation of ~3,000 m above sea-level and widespread Cenozoic alkaline basaltic volcanism (Hunt et al., 2012; Whitford-Stark, 1987; Windley & Allen, 1993). The southeastern section of the East Sayan region was primarily formed

19448007, 2025, 15, Downloaded from https://agupubs.onlinelibrary.wiley.com/doi/10.1029/2025GL117229 by Stephen Gao - Missouri University Of Science , Wiley Online Library on [30/07/2025]. See the Terms and Conditions (https://onlinelibrary.wiley.com/terms-and-conditions) on Wiley Online Library for rules of use; OA articles are governed by the applicable Creative Commons License

19448007, 2025, 15, Downloaded from https://agupubs.onlinelibrary.wiley.com/doi/10.1029/2025GL117229 by Stephen Gao - Missouri University Of Science , Wiley Online Library on [30/07/2025]. See the Terms and Conditions (https://onlinelibrary.wiley.com/terms-and-conditions) on Wiley Online Library for rules of use; OA articles are governed by the applicable Creative Commons License

during the Neoproterozoic-early Paleozoic era, marked by active processes involving island-arc development and accretion-collision events. Volcanic eruptions in the vicinity of the East Sayan region commenced during the Mid-Miocene epoch, specifically between 16 and 12 million years ago (Rasskazov, 1994). The Jom-Bolok volcanic field, situated in the southeastern region of the East Sayan Mountains range, was likely reactivated due to the combined influence of far-field tectonic stress from the India-Asia collision zone and extensional forces within the southwestern Baikal rift system (Ivanov & Demonterova, 2010; Molnar & Tapponnier, 1975). Volcanic activity peaked in Harmar Daban range (Figure 1) during the Miocene, with eruptions continuing locally into the Pleistocene, and this relatively recent event may be associated with the formation of the Baikal rift (Ionov et al., 1995). Some studies attribute the rapid rifting over the past 3–4 Ma to a thermal upwelling in the asthenosphere (Logatchev & Zorin, 1987) that is believed to have extended to the base of the crust in the expansive region east of Lake Baikal (Gao et al., 1994). However, studies on the formation mechanisms of magmatic activities in these relatively small volcanic fields remain limited and inconclusive (Ivanov et al., 2011).

The closure of the Mongol-Okhotsk ocean also has significant impact on the evolution of the deep structure beneath the Mongolia plateau and the Siberian craton (e.g., Dash et al., 2015; Tang et al., 2014). Previous seismic tomographic studies have imaged high velocity regions in the lower mantle which might represent remnants of the oceanic slab that was subducting northward under the Siberian craton (e.g., Van der Voo et al., 1999). Whether the subducted slab segments remain in the MTZ, and their possible influence on volcanisms remains enigmatic (Chen, Niu, Liu, & Tromp, 2015).

In this study, we stack a data set of 13,307 high-quality (as defined by signal to noise ratios specified in S. S. Gao and Liu, 2014b) P-to-s receiver functions (Figure S1 in Supporting Information S1) under the non-plane wave assumption (S. S. Gao & Liu, 2014a) recorded during 1990–2022 to obtain estimates of the depths of 410 and 660 km discontinuities beneath central Asia. The resultant depths of the MTZ discontinuities and thickness provide new evidence on the distribution of ancient subducted slab segments in the MTZ and formation mechanisms of Cenozoic volcanisms. We also suggest the presence of a lithospheric drip beneath the East Sayan Mountains that has reached the lower MTZ, probably triggered by a passing mantle plume that is currently located beneath the western tip of Lake Baikal as revealed by seismic tomography studies (Wu et al., 2021; Zhao et al., 2006). The existence of the drip is further supported by geochemical observations, a recent seismic tomography study indicating a high velocity zone in the lower MTZ (Lu et al., 2019), and lithospheric thickening directly associated with the drip and lithospheric thinning in surrounding areas (Pasyanos et al., 2014).

3. Data and Methods

3.1. Data Requesting

The broadband teleseismic data used in the study were recorded by 43 stations including permanent stations from the II network (active since 1990) and temporary stations in the XL array (for the period from 2012 to 2016) distributed in the area of 47°N to 52°N and 95°E to 105°E (Figure 1). All the seismograms were requested from the Seismological Facility for the Advancement of Geoscience (SAGE) Data Management Center (DMC). To balance the quantity and quality of the requested data, the epicentral distance range used for data request is from $\Delta_{min} = 30°$ to $\Delta_{max} = 100°$, and the cutoff magnitude (M_c) is defined by the epicentral distance (Δ) and focal depth (D) subjecting to the equation $M_c = 5.2 + (\Delta - \Delta_{min})/(\Delta_{max} - \Delta_{min}) - D/D_{max}$, where $D_{max} = 700$ km (Liu & Gao, 2010).

3.2. Data Processing

Data processing procedures used in this study are described in the SI section and S. S. Gao & Liu (2014b), and are briefly summarized here. The three-component seismograms are filtered utilizing a 4-pole, 2-pass Bessel filter with corner frequencies of 0.02 and 0.2 Hz. To attenuate the prominent PP phase, an exponential taper function with a half-width of 30 s is applied, centered on the theoretical PP arrival time. The frequency-domain water-level deconvolution algorithm (Ammon, 1991; Clayton & Wiggins, 1976) is implemented on the vertical component for selected seismograms that exhibit first-arrival signal-to-noise ratio (SNR) exceeding 4.0 to compute radial RFs. Following visual inspection, a total of 13,307 RFs displaying distinct initial P pulses from 5,026 events (Figure S1a in Supporting Information S1) are utilized in the analysis. The RFs are spatially grouped into circular bins with a radius of 0.5° based on the ray-piercing point coordinates (Figure 1) calculated at the midpoint of the MTZ (depth of 535 km). These binned RFs undergo moveout correction and stacking to generate depth profiles

19448007, 2025, 15, Downloaded from https://agupubs.onlinelibrary.wiley.com/doi/10.1029/2025GL117229 by Stephen Gao - Missouri University Of Science , Wiley Online Library on [30/07/2025]. See the Terms and Conditions (https://onlinelibrary.wiley.com/terms-and-conditions) on Wiley Online Library for rules of use; OA articles are governed by the applicable Creative Commons License

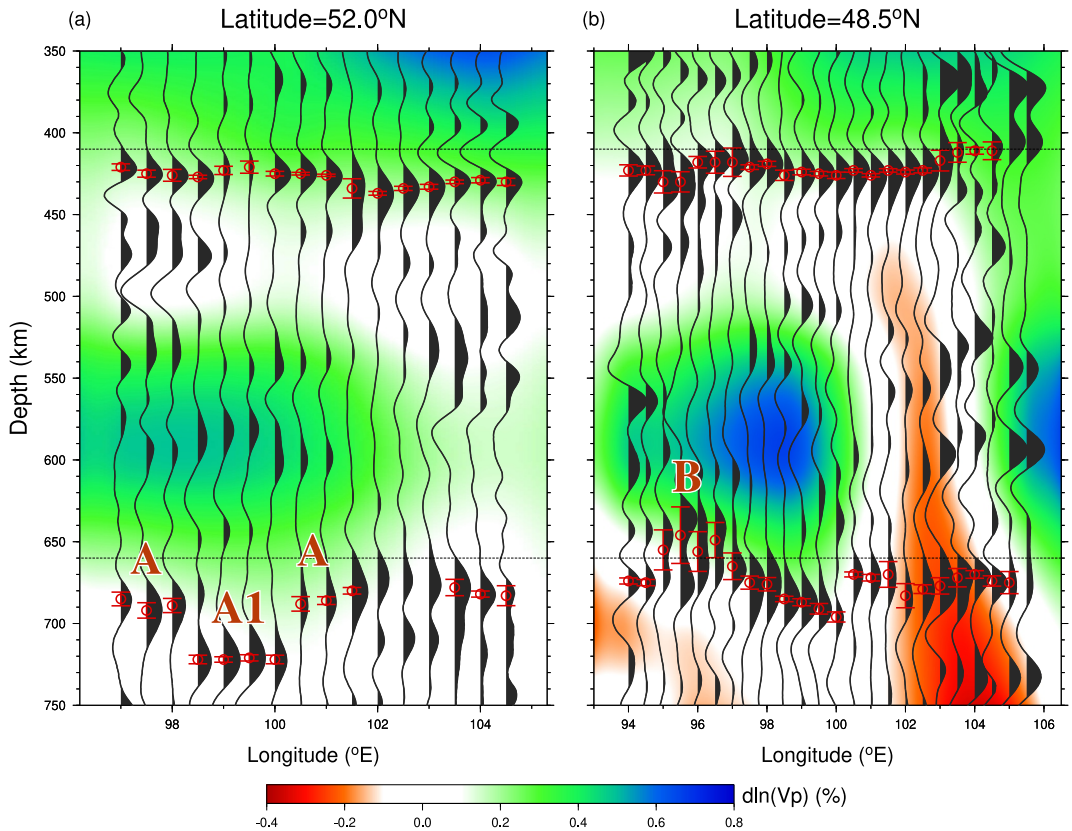

Figure 2. Stacked receiver functions along two latitudinal profiles. The mean depths and standard deviations for d410 and d660 are indicated by red circles and error bars, respectively. The background image displays P-wave velocity anomalies (Lu et al., 2019).

for each 0.5° interval. While the vast majority of the d410 and d660 arrivals are robust (Figure 2 and Figure S2 in Supporting Information S1), in a few instances, the depth windows are manually adjusted considering the depth and morphology of arrivals in adjacent bins. Specifically, if there are multiple arrivals with similar amplitudes, the one that shows the maximum similarity in the depth and waveform is selected. For a given bin, the mean depth for a MTZ discontinuity and the SD value are calculated using 50 bootstrap resampling iterations.

4. Results

4.1. Apparent Depths

The obtained MTZ discontinuity depths (Figure S3 and Table S1 in Supporting Information S1) using the aforementioned procedures are apparent rather than true depths due to the fact that the 1-D IASP91 Earth model is utilized in performing the moveout correction. Measurements for the d410 or d660 are obtained from 225 bins in total, including 217 bins for the d410, 214 bins for the d660 and 206 bins for both the d410 and d660. The measurements for each of the 225 bins can be found in Table S1 of Supporting Information S1. The spatially continuous resulting depths for the two MTZ discontinuities and the MTZ thickness are generated by applying a continuous curvature surface griding algorithm with a tension factor of 0.5 (Smith & Wessel, 1990).

Two sub-areas (A and B, Figure 3, Figure S3 and Table S2 in Supporting Information S1) display distinctive observations and thus are the focuses of the following discussions. Beneath Area A which is situated from the west to south of the Siberian craton, the d410 is apparently depressed by about 13 km and d660 is depressed about 30 km, leading to a MTZ thickness of 267 ± 13 km. Inside Area A, in the area marked as A1 (Figure 3), there is an area with greatly depressed d660. This area is located in the close vicinity of Cenozoic volcanic fields in the East Sayan Mountains (Figure 1). Beneath this area, the greatest MTZ thickening in the entire study area with an average thickness of 297 ± 5 km is detected, and the maximum thickness is about 302 km. The MTZ thickening is

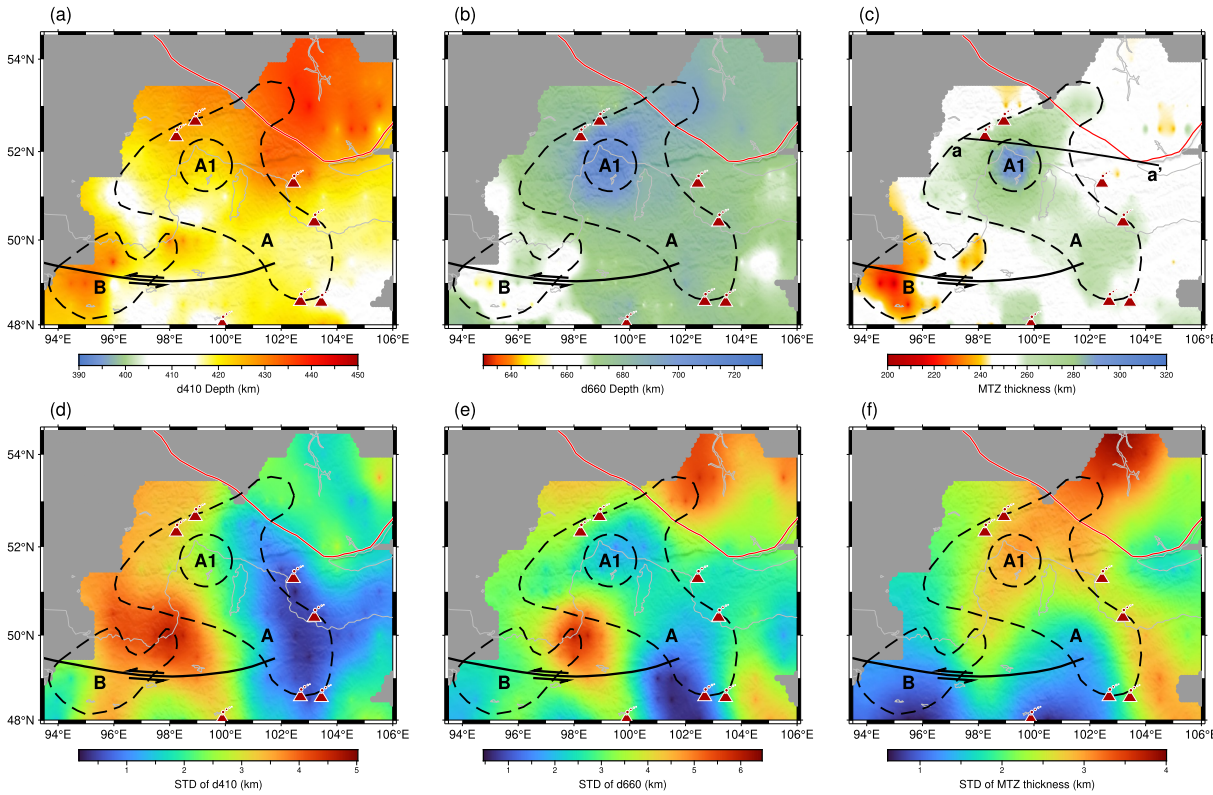

Figure 3. Spatial distribution of the averaged velocity corrected depths of d410 (a), d660 (b), and MTZ thickness (c). (d–f) One standard deviations (STDs) of the d410, d660 and MTZ thickness respectively. Profile a–a' in Panel (c) shows the approximate location of the schematic model shown in Figure 4.

mostly caused by the apparent depression of the d660 which corresponds to statistically significant positive amplitudes above the baseline (Figure 2a).

For Area B which includes the Tuva-Mongolian Massif, an apparent d410 depth of 433 ± 9 km and an apparent d660 depth of 662 ± 14 km are revealed, leading to an ~21 km MTZ thinning that is mostly caused by the depression of the d410 (Figure 2b). Relative to the adjacent bins, there is a slight shallowing of the d660 for the same bins with depressed d410 (Figure 2b).

4.2. Velocity Corrected Depths

The apparent depths are converted into velocity corrected depths by using two global (Lu et al., 2019; Obayashi et al., 2013) and three regional velocity models (Chen, Niu, Liu, Tromp, et al., 2015; Tao et al., 2018; Wu et al., 2021) according to the velocity correction procedure presented in S. S. Gao & Liu (2014a). The results can be found in Figure S4 of Supporting Information S1. Due to the significant disparity observed among these velocity models, we computed the average corrected d410 and d660 depths (Figure 3 and Table S3 in Supporting Information S1) for each bin from the five velocity models. The average corrected depths for Area A are 420 ± 6 km and 685 ± 14 km for d410 and d660, respectively, with a mean MTZ thickness of 265 ± 13 km. For Area A1, these values are 423 ± 2, 717 ± 4, and 294 ± 5 km; and for Area B, they are 428 ± 9, 657 ± 12, and 229 ± 11 km. The corrected results (Table S4 in Supporting Information S1) are within a few kilometers from the apparent measurements (Table S2 in Supporting Information S1) as a result of minor lateral variations in upper-mantle and MTZ velocities. As demonstrated in numerous receiver function studies of the MTZ, the corrected depths of the d410 and d660 are frequently positively correlated (e.g., S. S. Gao & Liu, 2014b). This is primarily due to insufficient correction of apparent depths, as the velocity anomaly amplitudes in most tomography models are lower than their true values due to the application of a spatial damping factor. Therefore, in the following discussion, we place greater emphasis on the corrected MTZ thickness rather than the individual corrected discontinuity depths.

19448007, 2025, 15, Downloaded from https://agupubs.onlinelibrary.wiley.com/doi/10.1029/2025GL117229 by Stephen Gao - Missouri University Of Science , Wiley Online Library on [30/07/2025]. See the Terms and Conditions (https://onlinelibrary.wiley.com/terms-and-conditions) on Wiley Online Library for rules of use; OA articles are governed by the applicable Creative Commons License

19448007, 2025, 15, Downloaded from https://agupubs.onlinelibrary.wiley.com/doi/10.1029/2025GL117229 by Stephen Gao - Missouri University Of Science , Wiley Online Library on [30/07/2025]. See the Terms and Conditions (https://onlinelibrary.wiley.com/terms-and-conditions) on Wiley Online Library for rules of use; OA articles are governed by the applicable Creative Commons License

5. Discussion

5.1. Constraining the Spatial Distribution of Slab Remnants in the MTZ

The spatial variations in MTZ thickness and the depths of seismic discontinuities provide key insights into the geometry and depth penetration of the slab segments beneath the region. For Area A, slab remnants from previous plate convergence such as the closure of the Paleo-Mongol-Okhotsk ocean and subduction of the Pacific plate beneath Eurasia (Chen, Niu, Liu, & Tromp, 2015) are possibly the main causes leading to the thickened MTZ. Under the assumption that the Clapeyron slope for the d410 is 2.9 MPa/K and that for the d660 is −1.3 MPa/K for the post-spinel transition (Fei et al., 2004), an MTZ thickening of 17 km corresponds to a positive temperature anomaly of 144 K. If a scale factor (dVp/dT) of -4.8×10^{-4} km s^{-1} K^{-1} (Deal et al., 1999) is used, a Vp velocity anomaly of about +0.75% is expected. Among the various tomography models (Figure S5 in Supporting Information S1), the one by Wu et al. (2021) fits the estimated value the best. In addition, the spatial distribution of the high velocities in this model (Figure S5e in Supporting Information S1) fits the area with thickened MTZ the best among all the models shown in Figure 3. It is important to note that, due to the wide range of previously reported Clapeyron slopes (Tauzin & Ricard, 2014) and the temperature-pressure dependence of the scale factor, the estimated temperature and velocity anomalies here and in the next section may carry significant uncertainties. However, these uncertainties do not impact the primary objective of this part of the study, which is to delineate the spatial distribution of thermal anomalies rather than their accurate amplitudes.

5.2. Possible Thermal Upwelling Beneath the Tuva-Mongolian Massif

A key feature of the observed MTZ discontinuity depths is the significant depression of the d410 by 23 km, while the d660 remains at a nearly normal (662 ± 14 km) depth beneath the Tuva-Mongolian Massif (Area B). After velocity corrections, the d410 is depressed by 18 km and the d660 is uplifted by 3 km. The MTZ beneath Area B is approximately 21 km thinner than the global average (Figure 3). Such a characteristic has been observed elsewhere such as SE Alaska (Dahm et al., 2017) and the NW Tibetan Plateau (Miao et al., 2024), and can be interpreted as thermal upwelling originating from inside the MTZ, which depresses the d410 but has no effect on the d660. In Area B, a viable mechanism for the deepening of the d410 is thermal upwelling associated with the western edge of the subducted Pacific slab. This interpretation is supported by a low-velocity zone (LVZ) that extends from the surface to the upper MTZ (Chen, Niu, Liu, Tromp, et al., 2015; Tao et al., 2018; Wu et al., 2021). Assuming a Clapeyron slope of +2.9 MPa/K for the d410 (Bina & Helffrich, 1994), the temperature anomaly near the d410 is calculated to be +220 K, and using the scaling factor of Deal et al. (1999), the corresponding velocity anomaly near the d410 is about −1.2%, which is approximately consistent with the velocity models of Tao et al. (2018) and Wu et al. (2021) (Figure S6 in Supporting Information S1).

5.3. Slab Dehydration as a Possible Cause for the Origin of Intraplate Cenozoic Volcanism

The spatial distribution of Cenozoic intraplate volcanism in the study region, encompassing the Jom-Bolok, Azas Plateau, Hamar-Daban Range, Dgida Basin, Khanuy Gol, and Orkhon Gol, predominantly coincides with the periphery of Area A. Such a spatial correspondence suggests that slab dehydration could be the ultimate cause of the Cenozoic volcanism. Mineral physics investigations indicate that subducting slabs older than 50 million years possess the capacity to deliver water into the MTZ through hydrous minerals and dense hydrous magnesium silicates, particularly hydrous ringwoodite, and phases E, D, and H (Pearson et al., 2014; Thompson, 1992). As temperature increases within these slabs, the water retention ability of wadsleyite and ringwoodite diminishes (Ohtani et al., 2004), thereby triggering continuous and prolonged dehydration processes. This process involves the release of volatiles from hydrous minerals within the slab as it undergoes phase transitions in the MTZ, potentially triggering flux melting in the overlying mantle wedge. Therefore, slab dehydration is a possible formation mechanism of the widespread recent magmatism in the peripheral regions of Area A (Figure 4).

5.4. A Possible Lithospheric Drip Traversing the MTZ

The greatest MTZ thickening is observed beneath the East Sayan Mountains, situated just south of the Azas Plateau and Jom-Bolok Cenozoic volcanic fields, with an average MTZ thickness of 297 ± 5 km within a circular region approximately 220 km in diameter (Area A1 in Figure 3). This thickening is primarily caused by a depression of the d660. Higher-than-normal seismic velocities are also observed in the lower MTZ beneath this area (Figure 2a). A thickened MTZ can result from either low temperatures associated with a subducted slab (Gu

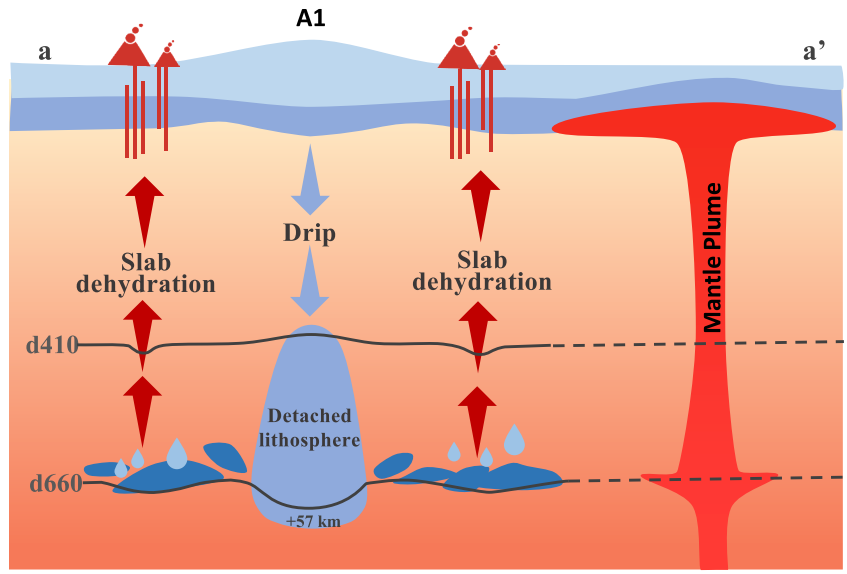

Figure 4. A cross-section diagram along Profile a–a' in Figure 3c to explain the main characteristics of the observations. The light-blue body represents lithospheric drip beneath the eastern Sayan Mountains, while the dark-blue objects indicate slab remnants. Blue arrows depict the downwelling movement of mantle lithosphere, and red arrows indicate the upward migration of hydrous fluids from slab dehydration processes.

et al., 1998) or elevated water content linked to older slab segments (Ghosh et al., 2013). Because high water content corresponds to lower-than-normal seismic velocities, which is not observed, we propose that the most plausible explanation for the nearly circular MTZ thickening in Area A1 is a lithospheric drip detaching into the lower MTZ, as detailed below.

Several independent observations support this interpretation. First, the presence of garnet-bearing minerals on the Azas Plateau points to an anhydrous mantle origin (Litasov et al., 2002), consistent with the expected geochemistry of a lithospheric drip rather than slab dehydration. Second, the Nb-Ta enrichment in local alkaline basalts suggests a high time-integrated 238U/204Pb (HIMU) component, indicative of recycled lithosphere (Aulbach et al., 2008; Litasov et al., 2002) and supports the involvement of an upwelling related to lithospheric dripping (Figure 4). Third, the anomalously thick lithosphere in Area A1, coupled with thin lithosphere in surrounding regions (Figure S7 in Supporting Information S1), can be explained by lithospheric material being drawn downward from adjacent areas. In contrast, the observed geometry and seismic characteristics do not favor a stalled subducted slab interpretation. Subducted slabs typically produce elongated zones of MTZ thickening, whereas the East Sayan anomaly is circular. Moreover, regions with elevated water content often correlate with negative seismic velocity anomalies, which are not observed here. Note that the strongest evidence supporting the lithospheric drip model is the thickened MTZ observed in this study within a circular-shaped area (Figure 3c), supplemented by geochemical observations. Although the circular lithospheric thickening shown in the Litho-1.0 global model (Figure S7 in Supporting Information S1) aligns well with the predicted geometry by the drip model, we acknowledge that the relatively low resolution of Litho-1.0 limits its ability to serve as definitive support on its own.

If we assume that (a) the drip was triggered by a passing mantle plume (Hales et al., 2005), (b) the commencement of volcanism during the Mid-Miocene epoch at about 16 Ma (Rasskazov, 1994) was associated with lithospheric thinning in areas surrounding the lithospheric drip, and (c) the Eurasian plate has been maintaining the current westward movement and 21 km/myr rate (Gripp & Gordon, 2002) since 16 Ma, we can estimate that the current location of the mantle plume is located about 350 km east of Area A1. Coincidentally, various seismic tomography studies (Wu et al., 2021; Zhao et al., 2006) have revealed a column of low seismic velocities extending from the MTZ to the uppermost mantle beneath the western Lake Baikal (Figure 1). The low velocities present an elliptical or circular shape and are interpreted as indicative of an active mantle upwelling. Furthermore, the region proposed as the current location of this plume is characterized by an anomalously thin lithosphere (Figure S7 in Supporting Information S1), providing additional evidence for the existence of the plume. Based on these

19448007, 2025, 15, Downloaded from https://agupubs.onlinelibrary.wiley.com/doi/10.1029/2025GL117229 by Stephen Gao - Missouri University Of Science , Wiley Online Library on [30/07/2025]. See the Terms and Conditions (https://onlinelibrary.wiley.com/terms-and-conditions) on Wiley Online Library for rules of use; OA articles are governed by the applicable Creative Commons License

observations, we suggest that the mantle plume now located beneath western Lake Baikal is the same entity responsible for the initiation of the lithospheric drip when Area A1 was directly above the plume several million years ago. Despite the seemingly strong supporting evidence from the circular-shaped MTZ thickness anomaly, seismic tomography, geochemical observations, lithospheric thickness estimates, and the apparent alignment of the proposed lithospheric drip with the "Baikal plume" and recent plate motion, a comprehensive geodynamic modeling effort is required to test the viability of the proposed drip model and to elucidate the interconnections among the various physical properties.

6. Conclusions

Integrating our receiver function observations with seismic tomography, lithospheric thickness and geochemical observations, this study proposes that remnants of the ancient slab reside in the lower MTZ beneath northern Mongolia, and intraplate magmatism in the area is potentially driven by slab dehydration. Mantle upwelling beneath the Tuva-Mongolian Massif is likely initiated by the subducted Pacific slab. Additionally, our findings indicate the presence of a lithospheric drip extending into the lower mantle beneath the East Sayan Mountains, likely triggered by interaction with a hot mantle plume currently located beneath western Lake Baikal.

Data Availability Statement

The seismological data utilized in this investigation are openly accessible through the Seismological Facility for the Advancement of Geoscience Data Management Center (https://ds.iris.edu/ds/nodes/dmc/), acquired via the BREQ_FAST data requisition protocol. The seismic waveform data set includes networks XL (Meltzer, 2012) and II (Scripps Institution of Oceanography, 1986). Specific data acquisition parameters, including the cut-off magnitude threshold and teleseismic distance range, are detailed in Section 3.1. Graphical representations were generated using Generic Mapping Tools versions 4.5.7 and 6.2.0 (Wessel et al., 2019; https://www.generic-mapping-tools.org/download/).

Acknowledgments

The teleseismic data used in the study are requested from the Seismological Facility for the Advancement of Geoscience (SAGE) Data Management Center (DMC). We thank Editor Daoyuan Sun and three anonymous reviewers for their constructive comments that greatly improved the manuscript. This study was supported by the United States National Science Foundation (Grants 1830644 to S. S. Gao & K.H. Liu, 1919789 to S.S. Gao, & 2149587 to K.H. Liu).

References

Ammon, C. J. (1991). The isolation of receiver effects from teleseismic P waveforms. *Bulletin of the Seismological Society of America*, *81*(6), 2504–2510. https://doi.org/10.1785/bssa0810062504

Aulbach, S., O'Reilly, S., Griffin, W., & Pearson, N. (2008). Subcontinental lithospheric mantle origin of high niobium/tantalum ratios in eclogites. *Nature Geoscience*, *1*(7), 468–472. https://doi.org/10.1038/ngeo226

Bina, C. R., & Helffrich, G. (1994). Phase transition clapeyron slopes and transition zone seismic discontinuity topography. *Journal of Geophysical Research*, *99*(B8), 15853–15860. https://doi.org/10.1029/94jb00462

Boyd, O. S., Jones, C. H., & Sheehan, A. F. (2004). Foundering lithosphere imaged beneath the southern Sierra Nevada, California, USA. *Science*, *305*(5684), 660–662. https://doi.org/10.1126/science.1099181

Camp, V. E., & Hanan, B. B. (2008). A plume-triggered delamination origin for the Columbia River basalt group. *Geosphere*, *4*(3), 480–495. https://doi.org/10.1130/GES00175.1

Chen, M., Niu, F., Liu, Q., & Tromp, J. (2015b). Mantle-driven uplift of Hangai Dome: New seismic constraints from adjoint tomography. *Geophysical Research Letters*, *42*(17), 6967–6974. https://doi.org/10.1002/2015gl065018

Chen, M., Niu, F., Liu, Q., Tromp, J., & Zheng, X. (2015). Multiparameter adjoint tomography of the crust and upper mantle beneath East Asia: 1. Model construction and comparisons. *Journal of Geophysical Research: Solid Earth*, *120*(3), 1762–1786. https://doi.org/10.1002/2014jb011638

Clayton, R., & Wiggins, R. A. (1976). Source shape estimation and deconvolution of teleseismic bodywaves. *Geophysical Journal International*, *47*(1), 151–177. https://doi.org/10.1111/j.1365-246x.1976.tb01267.x

Conrad, C. P., & Molnar, P. (1997). The growth of Rayleigh–Taylor-type instabilities in the lithosphere for various rheological and density structures. *Geophysical Journal International*, *129*(1), 95–112. https://doi.org/10.1111/j.1365-246X.1997.tb00939.x

Dahm, H. H., Gao, S. S., Kong, F., & Liu, K. H. (2017). Topography of the Mantle transition zone discontinuities beneath Alaska and its geodynamic implications: Constraints from receiver function stacking. *Journal of Geophysical Research: Solid Earth*, *122*(12). https://doi.org/10.1002/2017jb014604

Dash, B., Yin, A., Jiang, N., Tseveendorj, B., & Han, B. (2015). Petrology, structural setting, timing, and geochemistry of Cretaceous volcanic rocks in eastern Mongolia: Constraints on their tectonic origin. *Gondwana Research*, *27*(1), 281–299. https://doi.org/10.1016/j.gr.2013.10.001

Deal, M. M., Nolet, G., & van der Hilst, R. D. (1999). Slab temperature and thickness from seismic tomography: 1. Method and application to Tonga. *Journal of Geophysical Research*, *104*, 28789–28802. https://doi.org/10.1029/1999JB900255

DeCelles, P. G., Carrapa, B., Horton, B. K., McNabb, J. C., Gehrels, G. E., & Boyd, J. D. (2015). *The Miocene Arizaro Basin, central Andean hinterland: Response to partial lithosphere removal?* Geological Society of America eBooks. https://doi.org/10.1130/2015.1212(18)

Ducea, M. N., & Saleeby, J. B. (1998). A case for delamination of the deep batholithic crust beneath the Sierra Nevada, California. *International Geology Review*, *40*(1), 78–93. https://doi.org/10.1080/00206819809465199

Fei, Y., Van Orman, J., Li, J., van Westrenen, W., Sanloup, C., Minarik, W., et al. (2004). Experimentally determined postspinel transformation boundary in Mg_2SiO_4 using MgO as an internal pressure standard and its geophysical implications. *Journal of Geophysical Research*, *109*(B2). https://doi.org/10.1029/2003jb002562

Furman, T., Nelson, W. R., & Elkins-Tanton, L. T. (2016). Evolution of the East African rift: Drip magmatism, lithospheric thinning and mafic volcanism. *Geochimica et Cosmochimica Acta*, *185*, 418–434. https://doi.org/10.1016/j.gca.2016.03.024

19448007, 2025, 15, Downloaded from https://agupubs.onlinelibrary.wiley.com/doi/10.1029/2025GL117229 by Stephen Gao - Missouri University Of Science , Wiley Online Library on [30/07/2025]. See the Terms and Conditions (https://onlinelibrary.wiley.com/terms-and-conditions) on Wiley Online Library for rules of use; OA articles are governed by the applicable Creative Commons License

Gao, S., Davis, P. M., Liu, H., Slack, P. D., Zorin, Y. A., Logatchev, N. A., et al. (1994). Asymmetric upwarp of the asthenosphere beneath the Baikal rift zone, Siberia. *Journal of Geophysical Research*, *99*(B8), 15319–15330. https://doi.org/10.1029/94jb00808

Gao, S. S., & Liu, K. H. (2014a). Imaging mantle discontinuities using multiply-reflected P-to-S conversions. *Earth and Planetary Science Letters*, *402*, 99–106. https://doi.org/10.1016/j.epsl.2013.08.025

Gao, S. S., & Liu, K. H. (2014b). Mantle transition zone discontinuities beneath the contiguous United States. *Journal of Geophysical Research: Solid Earth*, *119*(8), 6452–6468. https://doi.org/10.1002/2014jb011253

Ghosh, S., Ohtani, E., Litasov, K. D., Suzuki, A., Dobson, D. P., & Funakoshi, K. (2013). Effect of water in depleted mantle on post-spinel transition and implication for 660 km seismic discontinuity. *Earth and Planetary Science Letters*, *371*(372), 103–111. https://doi.org/10.1016/j.epsl.2013.04.011

Göğüş, O. H., & Pysklywec, R. N. (2008). Near-surface diagnostics of dripping or delaminating lithosphere. *Journal of Geophysical Research*, *113*(11), 1–11. https://doi.org/10.1029/2007JB005123

Gripp, A. E., & Gordon, R. G. (2002). Young tracks of hotspots and current plate velocities. *Geophysical Journal International*, *150*(2), 321–361. https://doi.org/10.1046/j.1365-246x.2002.01627.x

Gu, Y. J., Dziewoński, A. M., & Agee, C. B. (1998). Global de-correlation of the topography of transition zone discontinuities. *Earth and Planetary Science Letters*, *157*(1–2), 57–67. https://doi.org/10.1016/s0012-821x(98)00027-2

Hales, T. C., Abt, D. L., Humphreys, E., & Roering, J. J. (2005). A lithospheric instability origin for Columbia River flood basalts and Wallowa Mountains uplift in Northeast Oregon. *Nature*, *438*(7069), 842–845. https://doi.org/10.1038/nature04313

Helffrich, G. (2000). Topography of the transition zone seismic discontinuities. *Reviews of Geophysics*, *38*(1), 141–158. https://doi.org/10.1029/1999rg000060

Houseman, G. A., McKenzie, D. P., & Molnar, P. (1981). Convective instability of a thickened boundary layer and its relevance for the thermal evolution of continental convergent belts. *Journal of Geophysical Research*, *86*(B7), 6115–6132. https://doi.org/10.1029/JB086iB07p06115

Hunt, A. C., Parkinson, I. J., Harris, N., Barry, T. L., Rogers, N., & Yondon, M. (2012). Cenozoic volcanism on the Hangai Dome, Central Mongolia: Geochemical evidence for changing melt sources and implications for mechanisms of melting. *Journal of Petrology*, *53*(9), 1913–1942. https://doi.org/10.1093/petrology/egs038

Ionov, D. A., O'Reilly, S. Y., & Ashchepkov, I. V. (1995). Feldspar-bearing Lherzolite xenoliths in alkali basalts from Hamar-Daban, southern Baikal region, Russia. *Contributions to Mineralogy and Petrology*, *122*(1), 174–190. https://doi.org/10.1007/s004100050120

Ito, E., & Katsura, T. (1989). A temperature profile of the mantle transition zone. *Geophysical Research Letters*, *16*(5), 425–428. https://doi.org/10.1029/gl016i005p00425

Ivanov, A. V., Arzhannikov, S. G., Demonterova, E. I., Arzhannikova, A. V., & Orlova, L. A. (2011). Jom-Bolok Holocene volcanic field in the East Sayan Mts., Siberia, Russia: Structure, style of eruptions, magma compositions, and radiocarbon dating. *Bulletin of Volcanology*, *73*(9), 1279–1294. https://doi.org/10.1007/s00445-011-0485-9

Ivanov, A. V., & Demonterova, E. I. (2010). Extension in the Baikal rift and the depth of basalt magma generation. *Doklady Earth Sciences*, *435*(2), 1564–1568. https://doi.org/10.1134/s1028334x10120032

Kay, R. W., & Kay, S. M. (1993). Delamination and delamination magmatism. *Tectonophysics*, *219*(1–3), 177–189. https://doi.org/10.1016/0040-1951(93)90295-U

Litasov, Y., Hasenaka, T., Litasov, K., Yarmolyuk, V., Sugorakova, A., Lebedev, V., & TaniguchiANIGUCHI, H. (2002). Petrologic characteristics of Cenozoic alkaline basalts from the Azas Plateau, northeast Tuva (Russia). *Tohoku University, Center for Northeast Asian Studies, Northeast Asian Studies*, *6*, 201–226.

Liu, K. H., & Gao, S. S. (2010). Spatial variations of crustal characteristics beneath the Hoggar swell, Algeria, revealed by systematic analyses of receiver functions from a single seismic station. *Geochemistry, Geophysics, Geosystems*, *11*(8). https://doi.org/10.1029/2010gc003091

Logatchev, N. A., & Zorin, Y. A. (1987). Evidence and causes of the two-stage development of the Baikal rift. *Tectonophysics*, *143*(1–3), 225–234. https://doi.org/10.1016/0040-1951(87)90092-8

Lu, C., Grand, S. P., Lai, H., & Garnero, E. J. (2019). TX2019SLab: A New P and S Tomography model incorporating subducting slabs. *Journal of Geophysical Research: Solid Earth*, *124*(11), 11549–11567. https://doi.org/10.1029/2019jb017448

McMillan, M., & Schoenbohm, L. M. (2023). Diverse styles of lithospheric dripping: Synthesizing gravitational instability models, continental tectonics, and geologic observations. *Geochemistry, Geophysics, Geosystems*, *24*(2). https://doi.org/10.1029/2022gc010488

Meltzer, A. (2012). Central Mongolia seismic experiment [Dataset]. *International Federation of Digital Seismograph Networks*. https://doi.org/10.7914/SN/XL_2012

Miao, Z., Gao, S. S., Sun, M., & Liu, K. H. (2024). Topography of the 410 and 660 km discontinuities beneath the Tibetan Plateau and adjacent areas. *Earth and Planetary Science Letters*, *644*, 118947. https://doi.org/10.1016/j.epsl.2024.118947

Molnar, P., & Tapponnier, P. (1975). Tectonics of Asia: Consequences and implications of a Continental collision. *Science*, *189*(4201), 419–426. https://doi.org/10.1126/science.189.4201.419

Obayashi, M., Yoshimitsu, J., Nolet, G., Fukao, Y., Shiobara, H., Sugioka, H., et al. (2013). Finite frequency whole mantle P wave tomography: Improvement of subducted slab images. *Geophysical Research Letters*, *40*(21), 5652–5657. https://doi.org/10.1002/2013gl057401

Ohtani, E., Litasov, K., Hosoya, T., Kubo, T., & Kondo, T. (2004). Water transport into the deep mantle and formation of a hydrous transition zone. *Physics of the Earth and Planetary Interiors*, *143–144*, 255–269. https://doi.org/10.1016/j.pepi.2003.09.015

Pasyanos, M. E., Masters, T. G., Laske, G., & Ma, Z. (2014). LITHO1.0: An updated crust and lithospheric model of the Earth. *Journal of Geophysical Research: Solid Earth*, *119*(3), 2153–2173. https://doi.org/10.1002/2013jb010626

Pearson, D. G., Brenker, F. E., Nestola, F., McNeill, J., Nasdala, L., Hutchison, M. T., et al. (2014). Hydrous mantle transition zone indicated by ringwoodite included within diamond. *Nature*, *507*(7491), 221–224. https://doi.org/10.1038/nature13080

Rapp, R. P., & Watson, E. B. (1995). Dehydration melting of metabasalt at 8–32 kbar: Implications for continental growth and crust-mantle recycling. *Journal of Petrology*, *36*(4), 891–931. https://doi.org/10.1093/petrology/36.4.891

Rasskazov, S. V. (1994). Magmatism related to the Eastern Siberia rift system and the geodynamics. *Bulletin des Centres de Recherches Exploration-Production Elf-Aquitaine*, *18*(2), 437–452.

Ringwood, A. E. (1975). *Composition and petrology of the Earth's mantle* (pp. 618). MacGraw-Hill.

Scripps Institution of Oceanography. (1986). Global seismograph network—IRIS/IDA [Dataset]. *International Federation of Digital Seismograph Networks*. https://doi.org/10.7914/SN/II

Shearer, P. M. (1991). Constraints on upper mantle discontinuities from observations of long-period reflected and converted phases. *Journal of Geophysical Research*, *96*(B11), 18147–18182. https://doi.org/10.1029/91jb01592

Smith, W. H. F., & Wessel, P. (1990). Gridding with continuous curvature splines in tension. *Geophysics*, *55*(3), 293–305. https://doi.org/10.1190/1.1442837

19448007, 2025, 15, Downloaded from https://agupubs.onlinelibrary.wiley.com/doi/10.1029/2025GL117229 by Stephen Gao - Missouri University Of Science , Wiley Online Library on [30/07/2025]. See the Terms and Conditions (https://onlinelibrary.wiley.com/terms-and-conditions) on Wiley Online Library for rules of use; OA articles are governed by the applicable Creative Commons License

Smyth, J. R., & Frost, D. J. (2002). The effect of water on the 410-km discontinuity: An experimental study. *Geophysical Research Letters*, *29*(10). https://doi.org/10.1029/2001gl014418

Tang, J., Xu, W., Wang, F., Wang, W., Xu, M., & Zhang, Y. (2014). Geochronology and geochemistry of Early–middle Triassic magmatism in the Erguna Massif, NE China: Constraints on the tectonic evolution of the Mongol–Okhotsk Ocean. *Lithos*, *184–187*, 1–16. https://doi.org/10.1016/j.lithos.2013.10.024

Tao, K., Grand, S. P., & Niu, F. (2018). Seismic structure of the upper mantle beneath Eastern Asia from full waveform seismic tomography. *Geochemistry, Geophysics, Geosystems*, *19*(8), 2732–2763. https://doi.org/10.1029/2018gc007460

Tauzin, B., & Ricard, Y. (2014). Seismically deduced thermodynamics phase diagrams for the mantle transition zone. *Earth and Planetary Science Letters*, *401*, 337–346. https://doi.org/10.1016/j.epsl.2014.05.039

Thompson, A. B. (1992). Water in the Earth's upper mantle. *Nature*, *358*(6384), 295–302. https://doi.org/10.1038/358295a0

van der Meijde, M., Marone, F., Giardini, D., & Van Der Lee, S. (2003). Seismic evidence for water deep in Earth's upper mantle. *Science*, *300*(5625), 1556–1558. https://doi.org/10.1126/science.1083636

van der Voo, R., Spakman, W., & Bijwaard, H. (1999). Mesozoic subducted slabs under Siberia. *Nature*, *397*(6716), 246–249. https://doi.org/10.1038/16686

Wessel, P., Luis, J. F., Uieda, L., Scharroo, R., Wobbe, F., Smith, W. H. F., & Tian, D. (2019). The Generic mapping tools version 6. *Geochemistry, Geophysics, Geosystems*, *20*(11), 5556–5564. https://doi.org/10.1029/2019GC008515

West, J. D., Fouch, M. J., Roth, J. B., & Elkins-Tanton, L. T. (2009). Vertical mantle flow associated with a lithospheric drip beneath the great Basin. *Nature Geoscience*, *2*(6), 439–444. https://doi.org/10.1038/ngeo526

Whitford-Stark, J. L. (1987). A survey of Cenozoic volcanism on mainland Asia. In *Special papers* (pp. 1–74). https://doi.org/10.1130/spe213-p1

Windley, B. F., & Allen, M. B. (1993). Mongolian Plateau: Evidence for a late Cenozoic mantle plume under central Asia. *Geology*, *21*(4), 295. https://doi.org/10.1130/0091-7613(1993)021

Wood, B. J., Pawley, A. R., & Suzuki, A. (1996). Water and carbon in the Earth´s mantle. *Philosophical Transactions of the Royal Society A*, *354*(1711), 1495–1511. https://doi.org/10.1098/rsta.1996.0060

Wu, H., Huang, Z., & Zhao, D. (2021). Deep structure beneath the southwestern flank of the Baikal rift zone and adjacent areas. *Physics of the Earth and Planetary Interiors*, *310*, 106616. https://doi.org/10.1016/j.pepi.2020.106616

Yamazaki, D., & Karato, S. (2001). Some mineral physics constraints on the rheology and geothermal structure of Earth's lower mantle. *American Mineralogist*, *86*(4), 385–391. https://doi.org/10.2138/am-2001-0401

Zandt, G. (2003). The southern Sierra Nevada drip and the mantle wind direction beneath the Southwestern United States. *International Geology Review*, *45*(3), 213–224. https://doi.org/10.2747/0020-6814.45.3.213

Zhao, D., Lei, J., Inoue, T., Yamada, A., & Gao, S. S. (2006). Deep structure and origin of the Baikal rift zone. *Earth and Planetary Science Letters*, *243*(3–4), 681–691. https://doi.org/10.1016/j.epsl.2006.01.033

References From the Supporting Information

Dueker, K. G., & Sheehan, A. F. (1997). Mantle discontinuity structure from midpoint stacks of converted P to S waves across the Yellowstone hotspot track. *Journal of Geophysical Research*, *102*(B4), 8313–8327. https://doi.org/10.1029/96jb03857

19448007, 2025, 15, Downloaded from https://agupubs.onlinelibrary.wiley.com/doi/10.1029/2025GL117229 by Stephen Gao - Missouri University Of Science , Wiley Online Library on [30/07/2025]. See the Terms and Conditions (https://onlinelibrary.wiley.com/terms-and-conditions) on Wiley Online Library for rules of use; OA articles are governed by the applicable Creative Commons License